journal

J. Am. Ceram. Soc., 89 [5] 1615–1620 (2006)
DOI: 10.1111/j.1551-2916.2006.00911.x


# Role of Rare-Earth Oxide Additives on Mechanical Properties and Oxidation Behavior of $Si_3N_4$/BN Fibrous Monolith Ceramics

Sigrun N. Karlsdottir† and John W. Halloran

Materials Science and Engineering Department, University of Michigan, Ann Arbor, Michigan 48109-2136

**The rare-earth oxides ytterbium oxide ($Yb_2O_3$) and lanthanum oxide ($La_2O_3$) were used as additives in fibrous monolithic (FM) $Si_3N_4$/BN composites to study their individual effect on flexural strength and oxidation behavior of the composite. Two compositions were prepared: 20 vol% BN/80 vol% $Si_3N_4$ with additives for the $Si_3N_4$ and BN being either 8 wt%$Yb_2O_3$ or 8 wt% $La_2O_3$. Four-point flexural testing and static oxidation experiments at 1400°C in dry air for 10 h were performed. The material with $Yb_2O_3$ showed a high flexural strength, graceful failure, and comparable strength to reported $Si_3N_4$/BN FMs with 6 wt% $Y_2O_3$ and 2 wt% $Al_2O_3$. The material with $La_2O_3$ showed lower flexural strength and brittle failure in the majority of the samples; this was believed to be related to the hydration of $La_2O_3$ from the rare-earth apatite phase, $La_5Si_3O_{12}N$, resulting in lanthanum hydrate crystals on the side surfaces of the samples and disintegration of the material. The surface of the FMLA sample after oxidation showed severe oxidation. In contrast, the oxidation test of the FMs with $Yb_2O_3$ revealed a thin oxide scale containing small $Yb_2Si_2O_7$ on the $Si_3N_4$ cells but large $Yb_2Si_2O_7$ on the BN cell boundary. Also, microscopic analysis showed ~100 μm recession in the BN cell boundary and an ~4 μm oxide scale on $Si_3N_4$ cells.**

## I. Introduction

FIBROUS MONOLITHIC (FM) ceramics are laminates with a 3D structure. Because of their unique structure, they fail in a non-catastrophic way and thus have been considered as promising materials for structural applications.[1–5] FM ceramics have a fibrous texture and consist of a strong cell surrounded by a weaker boundary phase. The most thoroughly investigated FM ceramic system is the $Si_3N_4$/BN FMs.[1–8] This system is considered one of the most promising FMs because of its high strength at elevated temperatures and thermal shock resistance.[3–6] The additives yttrium oxide ($Y_2O_3$) and aluminum oxide ($Al_2O_3$) are conventionally used in the cells of the $Si_3N_4$ in the $Si_3N_4$/BN FMs as sintering aids. It is well known that during sintering of monolithic $Si_3N_4$ (containing sintering additives), a liquid phase forms when the sintering additives react with $SiO_2$ that coats the $Si_3N_4$ particles. After sintering, this liquid phase is usually retained in a glassy intergranular phase.[9,10] For $Si_3N_4$/BN FMs with $Y_2O_3$ and $Al_2O_3$ as additives, the glassy phase forms and is known to migrate into the BN cell boundaries during hot pressing.[2,4] This intergranular glassy phase influences the mechanical properties of the $Si_3N_4$/BN FMs at elevated temperatures.[3]

In an effort to enhance the mechanical properties of monolithic $Si_3N_4$ at room temperature and at elevated temperatures, many researchers have added sintering additives to $Si_3N_4$ to increase the refractoriness of the glassy intergranular phase and/or crystallize the grain–boundary phase.[11–15] Liu and Nemat-Nasser[12] studied the microstructure of an *in situ* reinforced silicon nitride, sintered with the rare-earth oxides lanthanum oxide ($La_2O_3$) and $Y_2O_3$. They found crystalline grain–boundary phases $La_5Si_3O_{12}N$ and $Y_5Si_3O_{12}N$, formed at grain pockets and two grain boundaries of the $Si_3N_4$. Cinibulk *et al.*[13,14] achieved good oxidation resistance and mechanical properties of monolithic $Si_3N_4$ at high temperatures by sintering the $Si_3N_4$ with various rare-earth oxides and silicon dioxide additives and then heat treated it to form crystalline rare-earth silicate phases. Park *et al.*[15] used $Yb_2O_3$ as a sintering aid to enhance the mechanical properties of $Si_3N_4$. They found that the amount of $Yb_2O_3$ had considerable effects on the microstructural evolution and the composition of the secondary phase in the grain boundary. Different crystalline grain boundary phases were formed for different amounts of $Yb_2O_3$; for 8 wt% $Yb_2O_3$ crystalline $Yb_2Si_2O_7$ was formed at the grain boundary along with a glassy phase. The size of the $Si_3N_4$ grains also varied with the amount of $Yb_2O_3$. These changes influenced the mechanical properties of the material at room temperature and elevated temperature, i.e. the flexural strength increased with the increased amount of $Yb_2O_3$ used.

Other researchers have used sintering additives in $Si_3N_4$ to increase oxidation resistance. Lee and Readey[16] increased the oxidation resistance of $Si_3N_4$ by using $Yb_2O_3$ as an additive and then generating a protective ytterbium silicate ($Yb_2Si_2O_7$) skin by a controlled oxidation process associated with the reaction between the $Si_3N_4$ oxidation products SiO2 and $Yb_2O_3$. $Yb_2Si_2O_7$ has also been reported as one of the main oxidation products formed on the surface of nanocomposite $Si_3N_4$–SiC with $Yb_2O_3$ as a sintering additive.[17]

Just as rare-earth oxides have been shown to confer suitable grain boundary properties to $Si_3N_4$ and enhance mechanical properties and oxidation resistance, rare-earth oxides can be expected to confer suitable grain boundary properties to the $Si_3N_4$ cell for the $Si_3N_4$/BN FMs and also possibly increase the stability of the BN cell boundary phase at elevated temperatures. However, so far, no research has been carried out on this aspect. In this paper, we investigated the mechanical properties and oxidation behavior of $Si_3N_4$/BN FMs with the rare-earth oxide additives, $Yb_2O_3$ and $La_2O_3$, by flexural strength testing at room temperature and static oxidation testing at 1400°C in dry air for 10 h.

## II. Experimental Procedure

### (1) Material Fabrication

FM $Si_3N_4$/BN samples were fabricated firstly by using coextrusion to prepare green filaments. The filaments were then stacked to form a green billet. After a binder burnout step, the billets were hot pressed at 25 MPa for 1 h in a flowing $N_2$ atmosphere at 1800°C. Detailed descriptions of the fabrication of FMs have been further described elsewhere.[1]

Billets with two different compositions were prepared: 20 vol% BN/80 vol% $Si_3N_4$ with additives for the $Si_3N_4$ and BN being either 8 wt%- $Yb_2O_3$ (REacton, Alfa Aesar, Ward Hill, MA) or 8 wt% $La_2O_3$. Lanthanum hydrate, $La(OH)_3$ (Alfa Aesar), was

M. Cinibulk—contributing editor

Manuscript No. 20810. Received July 27, 2005; approved November 29, 2005.
†Author to whom correspondence should be addressed. e-mail: nanna@umich.edu

**Table I. Composition and Densities of the fabricated $Si_3N_4$/BN FMs**

| | Ytterbium oxide (wt%) | Lanthanum oxide (wt%) | Measured ρ (g/cm$^3$) | Theoretical ρ (g/cm$^3$) |
|---|---|---|---|---|
| FMYB | 8 | — | 3.09±0.1 | 3.16 |
| FMLA | — | 8 | 2.95±0.1 | 3.12 |

used in place of the reactive $La_2O_3$. Heating $La(OH)_3$ in dry air led to a progressive dehydration of the $La(OH)_3$ to $La_2O_3$.[18] In our fabrication, the $La(OH)_3$ then dehydrated during hot pressing and transformed into $La_2O_3$. Both billets consisted of filaments stacked up, forming a 3D structure with ~250 μm $Si_3N_4$ cells (M11, H.C. Starck, MA) uniaxially aligned and separated by ~15 μm BN cell boundaries (6003, Advanced Ceramics Corp., OH). The densities of the specimens were measured using the Archimedes method, and the theoretical density of the specimen was estimated by the rule of mixture where the vol% of the BN phase was estimated to be 20 and the $Si_3N_4$ phase to be 80. The densities and compositions of the billets are shown in Table I.

### *(2) Flexural Testing*

Flexural bars were prepared for four-point flexural testing. The billets were first ground with a 220 grit—diamond wheel and then cut into 2.2 mm × 4.2 mm × 49 mm bars. The sides of the bars were chamfered to minimize machining flaws. The tensile sides of the bars were polished down to 1 μm using a medium polishing diamond disk. The flexural strength was measured at room temperature in laboratory air using a computer-controlled, screw-driven, testing machine (Model 4483, Instron Corp., Canton, MA). The specimens were tested using a four-point flexural testing fixture with an inner and an outer span of 20 and 40 mm and at a cross-head speed of 0.5 mm/min. Load versus cross-head deflection response and work of fracture (WOF) are reported here. Flexural strength is defined as the apparent flexural stress at load drop. Energy absorption capability is characterized by the WOF, calculated by determining the area under the load–cross-head deflection curve and dividing it by twice the cross-sectional area of the sample. Scanning electron microscopy (SEM) was used for examining crack deflection, and delamination cracking and sliding on the side surfaces of the tested flexural bars.

### *(3) Oxidation Testing*

Oxidation studies were conducted in a vertical tube furnace at 1400°C in dry air for 10 h. The furnace was heated at a heating rate of 100°C/min and then maintained at 1400°C for 10 h. Before oxidation of the samples, 2.2 mm × 4.2 mm × 20 mm bars were polished down to 1 μm using a medium polishing diamond disk. The specimens were then ultrasonically cleaned in acetone and dried before oxidation. The materials were characterized by X-ray diffractometry (XRD) before and after the oxidation test. The composition and morphology of an oxide layer produced after oxidation were characterized by SEM and X-ray energy-dispersive spectroscopy (XEDS).

## III. Results and Discussion

### *(1) Mechanical Properties*

FMs are laminates and can fail in two different modes during flexural testing by shear initiation, where the shear stress between the inner and outer loading pins in the middle of the beam exceeds the shear strength of the material, and by tensile initiation, where the tensile stress in the outer layer of the tensile surface exceeds the tensile strength of the material. Here, we report fracture of the FMs by two modes: tensile initiation and shear initiation. Table II gives the average strength and WOF of

**Table II. Flexural Strength and WOF of $Si_3N_4$/BN FMs with Ytterbium oxide (FMYB) and $Si_3N_4$/BN FMs with Lanthanum oxide (FMLA)**

| | Stress (MPa) | Work-of-fracture (J/m$^2$) |
|---|---|---|
| FMYB | | |
| Average | 340 | 2126 |
| Standard | 91 | 940 |
| FMLA | | |
| Average | 298 | 1287 |
| Standard | 61 | 384 |

the FMLA and FMYB samples. The $Si_3N_4$/BN FMs with $Yb_2O_3$ showed average high flexural strength and graceful failure and comparable strength of commercially available uniaxially $Si_3N_4$/BN FMs with 6 wt% $Y_2O_3$ and 2 wt% $Al_2O_3$, with the average flexural strength reported as 510±87 MPa.[4] On the other hand, the $Si_3N_4$/BN FMs with $La_2O_3$ showed lower flexural strength and brittle failure in the majority of the samples. The FMYB had 97.8% theoretical density and FMLA had 94.6% theoretical density; this is not believed to be a large enough difference to explain completely the poor mechanical behavior of the FMLA samples. Figure 1 shows an example of a flexural response, a graceful failure, of the FMYB sample in a stress versus cross-head displacement curve. The apparent peak stress was 448 MPa and there was a large load drop where the retained apparent stress was ~50 MPa and the WOF was 3037 J/m$^2$. Figure 2 shows an SEM micrograph of the side view of the corresponding FMYB sample, where the tensile initiation of the fracture can be seen along with crack deflection and subsequent delamination cracking and sliding along the side surface. The two fracture modes, tensile and shear initiation, were observed for both the FMYB and FMLA samples. Figure 3 shows an example of stress versus cross-head displacement curve of an FMLA sample that fractured by shear initiation and failed gracefully. The apparent peak stress was 233 MPa for this sample and the load drop was less compared with the tensile-initiated fracture shown in Fig. 1. The retained apparent stress was ~160 MPa and the WOF was 1304 J/m$^2$. Figure 4 shows the side view of the corresponding FMLA sample where the shear failure initiated in the flexural bar between the outer and inner loading pins. The entire shear-initiated fractured samples had higher retained apparent stress than the tensile-initiated fracture samples. It was observed that all the samples that failed gracefully (non-catastrophically) required extensive crack interaction such as crack deflection, delamination cracking, and sliding. The average WOF for FMLA was lower than for the FMYB (Table II) because of the fact that the majority of the FMLA samples fractured in a brittle manner and therefore there was fewer delamination and crack deflection, resulting in less energy

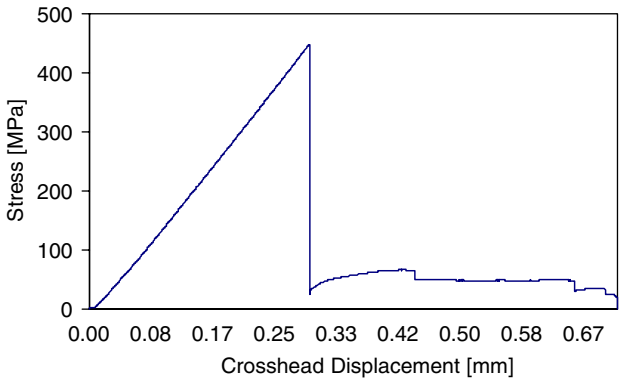


**Fig. 1**. Flexural response of $Si_3N_4$/BN FMs with ytterbium oxide (FMYB).

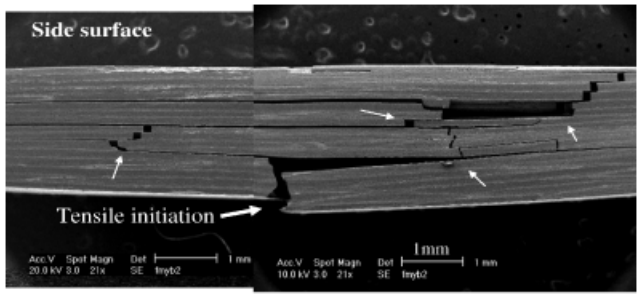


**Fig. 2**. Scanning electron micrograph of a side view of an FMYB flexural bar showing a tensile initiated fracture.

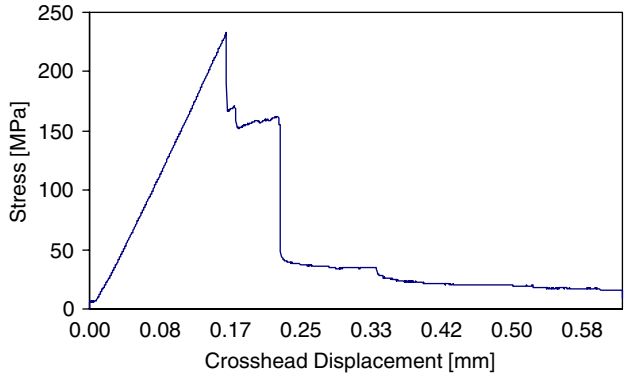


**Fig. 3**. Flexural response of $Si_3N_4$/BN FMs with lanthanum oxide (FMLA).

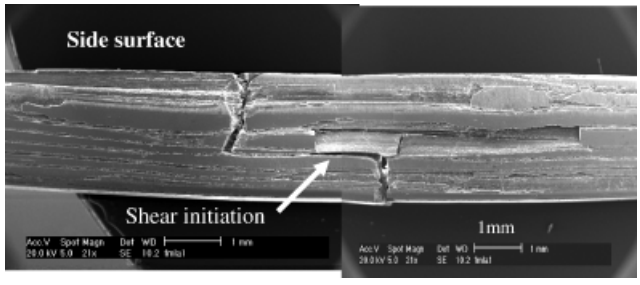


**Fig. 4**. Scanning electron micrograph of a side view of an FMLA flexural bar showing a shear-initiated fracture, between the outer and inner loading pins.

dissipation. During an SEM/XEDS procedure, lanthanum-rich crystals were observed spread over the side surfaces of the FMLA specimens; see Fig. 5. XEDS analyses of these crystals showed peaks of N, O, Si, and La. XRD analyses were also performed, where β-$Si_3N_4$, BN, and small rare-earth apatite $La_5Si_3O_{12}N$ phases were identified. The rare-earth apatite phase, $La_5Si_3O_{12}N$, was identified in grain–boundary phases in an *in situ* reinforced silicon nitride with $La_2O_3$.[12] The composition of the lanthanum-rich crystals growing from the side surfaces was believed to be $La(OH)_3$ crystals that were formed in air during hydration of $La_2O_3$ from the rare-earth apatite phase, $La_5Si_3O_{12}N$. This could not be confirmed with XRD analysis because of the small amount of the crystals on the samples. Meadowcroft[19] found that a strontium-doped lanthanum chromite prepared to comprise $LaCrO_3+x$ mol% SrO disintegrated at room temperature, owing to the formation of $La(OH)_3$, which was established by XRD analysis. The strontium was believed to have displaced the lanthanum in order to dope the lanthanum chromite, and then the free $La_2O_3$ hydrated with time, where the associated expansion caused the ceramic to disintegrate. The brittle behavior and low strength of the FMLA samples compared with the FMYB samples also gave us reason to believe that the ceramic disintegrated because of hydration of $La_2O_3$, available from the rare-earth apatite phase, $La_5Si_3O_{12}N$.

### *(2) Characterization of the Oxidation Surface Layer*

The surface of the FMLA sample after oxidation for 10 h at 1400°C in dry air showed severe oxidation; SEM analysis of the surface of the sample showed that the oxidation layer was covered with burst bubbles and cracks. Because of the disintegration of the FMLA samples, we will not discuss the oxidation of the FMLA here in this paper but will focus on the oxidation of the FMYB.

The oxidation behavior of $Si_3N_4$ ceramics with additive systems has been reported to be strongly dependent on the chemical composition of the oxidation surface layer formed by the oxidation products of the $Si_3N_4$ and the sintering additives.[20] Figure 6(a) shows an SEM picture of the top view of the oxidized surface of FMYB after 10 h at 1400°C in dry air where an oxide scale has formed. With XEDS and X-ray diffractiometry, the oxidation product was identified to be mainly ytterbium silicates ($Yb_2Si_2O_7$). Large ytterbium silicates, ~20 μm, were found on the BN cell boundary but small ytterbium silicates were found on the $Si_3N_4$ cells of ~0.8 μm. This can be seen in Figs. 6(b) and (c), which shows a higher magnification of the ytterbium silicates on the BN boundary phase and the $Si_3N_4$ cells in Fig. 6(a); the ytterbium silicates are the white flattened crystals in Figs. 6(a)–(c). XRD was performed before and after the oxidation testing for FMYB. The XRD analysis of the unoxidized FMYB sample revealed β-$Si_3N_4$, BN, and $Yb_4Si_2O_7N_2$ peaks, and β-$Si_3N_4$, BN, $Yb_4Si_2O_7N_2$, and $Yb_2Si_2O_7$ peaks of

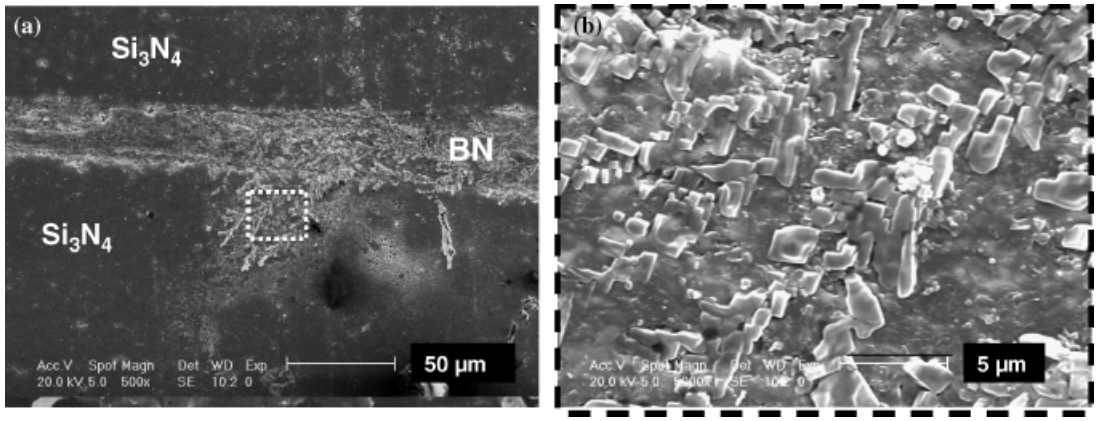


**Fig. 5**. (a) Lanthanum-rich crystals formed on the side surface of FMLA samples. (b) Magnification of the box in (a) of the crystals formed.

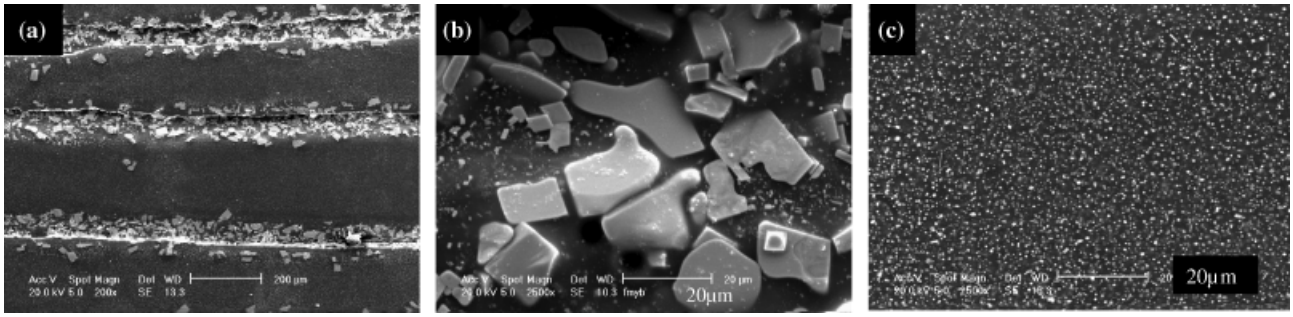


**Fig. 6**. (a) Oxidized surface of FMYB after 10 h at 1400°C in dry air. Large ytterbium silicates are apparent on the BN cell boundary phase; (b) magnification of the BN boundary phase in (a) showing large ytterbium silicates; and (c) magnification of a $Si_3N_4$ cell showing small ytterbium silicates on the surface.

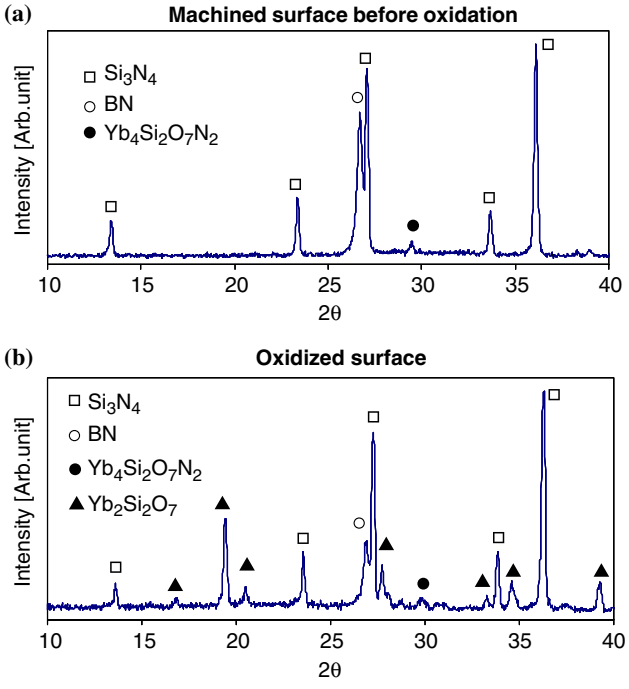


**Fig. 7**. X-ray diffraction pattern of the surface of the FMYB before (a) and after (b) oxidation.

the oxidized FMYB sample; see Fig. 7. By comparing the two diffraction patterns, it is evident that there was considerable formation of ytterbium silicates ($Yb_2Si_2O_7$) during the oxidation and a decrease in the BN phase after the oxidation; see Fig. 7.

It is well known that during oxidation of $Si_3N_4$, a silica ($SiO_2$) film is formed on the surface of the $Si_3N_4$. If there are any oxides used as sintering additives in the $Si_3N_4$ phase the $SiO_2$ forms an oxide layer on the surface after reacting with the sintering additives.[14,16,21] For $Si_3N_4$ with $Y_2O_3$ as a sintering additive, the oxide layer has been reported to consist of yttrium silicates ($Y_2Si_2O_7$), which is the most stable compound in the Y–Si–O system.[21–23] $Yb_2Si_2O_7$ skin has been reported to form on $Si_3N_4$ containing $Yb_2O_3$ as a sintering additive by a controlled oxidation process associated with the reaction between the $SiO_2$ and $Yb_2O_3$.[16] $Yb_2Si_2O_7$ has also been reported as one of the main oxidation products formed on the surface of nanocomposite $Si_3N_4$–SiC with $Yb_2O_3$ as a sintering additive.[17]

Here, we have a 3D composite consisting of two different ceramic materials: $Si_3N_4$ cells aligned in the uniaxial direction and a BN cell boundary phase separating the $Si_3N_4$ cells. $Si_3N_4$ with $Y_2O_3$ and $Al_2O_3$ as sintering additives have been shown oxidize at 1100°–1200°C,[21,23] but BN starts oxidizing at lower temperatures; generally, the onset of measurable oxidation is about 800°C, but tends to decrease with higher oxygen impurity levels within the BN. At 800°C the BN starts to oxidize into a liquid oxide ($B_2O_3$) by the oxidation reaction[24,25]:

$$2BN(s) + \frac{3}{2}O_2(g) = B_2O_3(l) + N_2(g)$$

The $B_2O_3$ liquid oxide is believed to start volatilizing at temperatures above 1100°C.[26]

The BN cell boundary phase in the FMYB sample consists of BN grains surrounded by a glassy phase that migrates into the boundary phase during hot pressing. This can be seen from Fig. 8, where the bright white spots represent the glassy phase between the BN platelets, while the gray phase is the BN platelets. After the oxidation testing on the FMYB sample, there was an ~100 μm recess at the BN cell boundary while there was an ~4 μm oxide layer on $Si_3N_4$ cells, and the oxidation zone was uniformly distributed around the surface; see Figs 9 and 10.

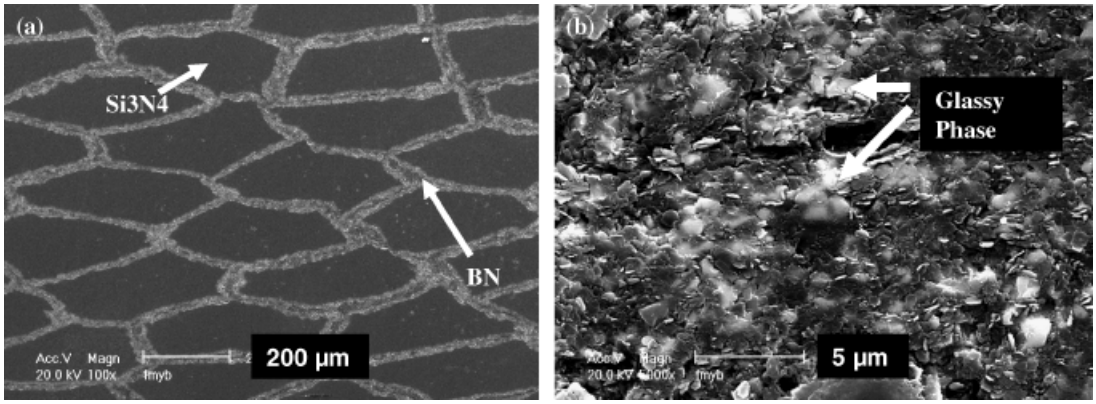


**Fig. 8**. (a) Microstructure of the FMYB sample consisting of BN cell boundary phases and $Si_3N_4$ cells. (b) Magnification of the BN cell boundary, that consists of BN grains surrounded by a glassy phase that migrated into the boundary phase during hot pressing.

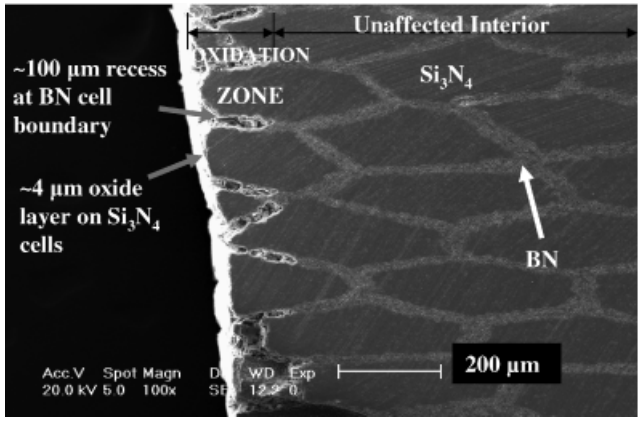


**Fig. 9**. FMYB sample after oxidation at 1400°C for 10 h. The oxidation zone was uniformly distributed around the surface.

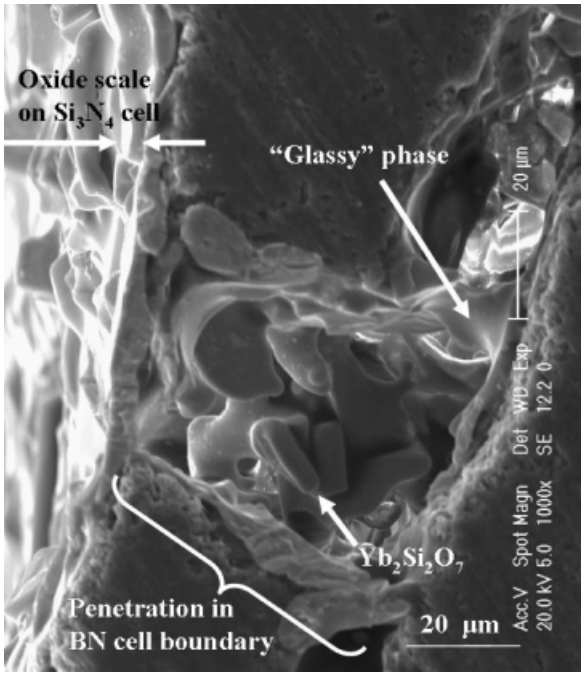


**Fig. 10**. Side view of a cross-section of an FMYB sample showing the BN boundary phase after oxidation.

Thus, the BN cell boundaries started to oxidize before the $Si_3N_4$ cells, where the BN grains in the cell boundary started to oxidize into liquid oxide ($B_2O_3$). The $B_2O_3$ liquid oxide then started to volatize at higher temperatures and yielded $Yb_2Si_2O_7$ and left behind some residue of the amorphous glassy phase; see Fig. 10.

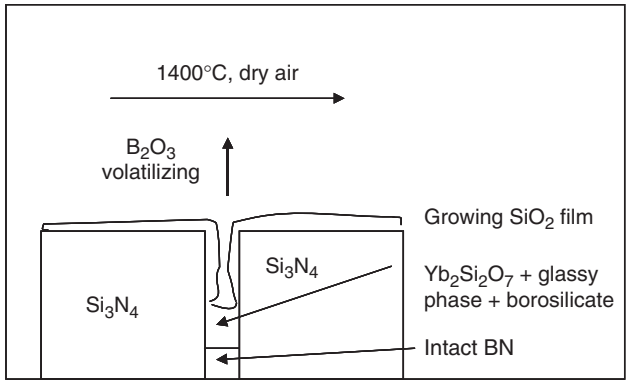


**Fig. 11**. Schematic of the oxidation process for the exposed $Si_3N_4$ cells and BN boundary phase.

The reason why larger $Yb_2Si_2O_7$ were found in the BN cell boundary than on the surface of the $Si_3N_4$ cells is that the boro-silicate glass in the boundary phase has a lower viscosity than the glass in the grain–boundary phases, thus allowing more rapid diffusion and thus larger $Yb_2Si_2O_7$ grains emanated from the BN boundary phases than from the $Si_3N_4$ cells. Figure 11 shows a schematic diagram of the oxidation mechanism of the FMYB.

## IV. Conclusion

The $Si_3N_4$/BN FM with 8 wt% $Yb_2O_3$ showed a flexural strength of $340 \pm 91$ MPa and graceful failure with a WOF of $2126 \pm 940$ J/m$^2$. These properties are comparable with reported $Si_3N_4$/BN FMs with 6 wt% $Y_2O_3$ and 2 wt% $Al_2O_3$. The oxidation test of the FMs with $Yb_2O_3$ revealed a thin oxide scale containing small $Yb_2Si_2O_7$ on the $Si_3N_4$ cells but large $Yb_2Si_2O_7$ on the BN cell boundary. Also, microscopic analysis after the oxidation test showed an $\sim$100 μm recess in the BN cell boundary and an $\sim$4 μm oxide scale on $Si_3N_4$ cells, uniformly distributed around the surface of the sample.

The $Si_3N_4$/BN FMs with $La_2O_3$ showed a flexural strength of $298 \pm 90$ MPa and brittle failure in the majority of the samples. The brittle behavior and low strength of the FMLA samples compared with the FMYB samples were believed to be due to disintegration of the sample, because of the hydration of $La_2O_3$ from the rare-earth apatite phase, $La_5Si_3O_{12}N$. The surface of the FMLA sample after oxidation for 10 h at 1400°C in dry air showed severe oxidation.

In conclusion, the $Si_3N_4$/BN FM with $Yb_2O_3$ as a sintering additive has proven to be similar in strength at room temperature to the commercially available $Si_3N_4$/BN FMs with 6 wt% $Y_2O_3$ and 2 wt% $Al_2O_3$, and to have a promising oxidation behavior. The rare-earth sintering aid, $La_2O_3$, has shown not to confer suitable mechanical properties or oxidation resistance to $Si_3N_4$/BN FMs.

## References

[1]S. Baskaran, S. D. Nunn, D. Popovic, and J. W. Halloran, "Fibrous Monolithic Ceramics: I, Fabrication, Microstructure, and Indentation Behavior," *J. Am. Ceram. Soc.*, **76** [9] 2209–16 (1993).

[2]D. Kovar, B. H. King, R. W. Trice, and J. W. Halloran, "Fibrous Monolithic Ceramics," *J. Am. Ceram. Soc.*, **80** [10] 2471–87 (1997).

[3]R. W. Trice and J. W. Halloran, "Elevated-Temperature Mechanical Properties of Silicon Nitride/Boron Nitride Fibrous Monolithic Ceramics," *J. Am. Ceram. Soc.*, **83** [2] 311–6 (2000).

[4]R. W. Trice and J. W. Halloran, "Effect of Sintering Aid Composition on the Processing of $Si_3N_4$/BN Fibrous Monolithic Ceramics," *J. Am. Ceram. Soc.*, **82** [11] 2943–7 (1999).

[5]R. W. Trice and J. W. Halloran, "Influences of Microstructure and Temperature on the Interfacial Fracture Energy of Silicon Nitride/Boron Nitride Fibrous Monolithic Ceramics," *J. Am. Ceram. Soc.*, **82** [9] 2502–8 (1999).

[6]Y.-H. Koh, H.-W. Kim, H.-E. Kim, and J. W. Halloran, "Thermal Shock Resistance of Fibrous Monolithic $Si_3N_4$/BN Ceramics," *J. Eur. Ceram. Soc.*, **24**, 2339–47 (2004).

[7]K. C. Goretta, F. Gutierrez-Mora, N. Chen, J. L. Routbort, T. A. Orlova, B. I. Smirnov, and A. R. de Arellano-Lopéz, "Solid-Particle Erosion and Strength Degradation of $Si_3N_4$/BN Fibrous Monoliths," *Wear*, **256**, 233–42 (2004).

[8]M. Y. He, D. Singh, J. C. McNulty, and F. W. Zok, "Thermal Expansion of Unidirectional and Cross-Ply Fibrous Monoliths," *Compos. Sci. Technol.*, **62**, 967–76 (2002).

[9]D. R. Clarke and G. Thomas, "Grain Boundary in a Hot-Pressed MgO Fluxed Silicon Nitride," *J. Am. Ceram. Soc.*, **60** [11–12] 491–5 (1977).

[10]D. R. Clarke, "On the Equilibrium Thickness of Intergranular Glass Phases in Ceramic Materials," *J. Am. Ceram. Soc.*, **70** [1] 15–22 (1987).

[11]Y. Goto and G. Thomas, "Microstructure of Silicon Nitride Ceramics Sintered with Rare-Earth Oxides," *Acta Metall. Mater.*, **43** [3] 923–30 (1995).

[12]M. Liu and S. Nemat-Nasser, "The Microstructure and Boundary Phases of In-Situ Reinforced Silicon Nitride," *Mater. Sci. Eng.*, **A254**, 242–52 (1998).

[13]M. K. Cinibulk, G. Thomas, and S. M. Johnson, "Strength and Creep Behavior of Rare-Earth Disilicate–Silicon Nitride Ceramics," *J. Am. Ceram. Soc.*, **75** [8] 2050–5 (1992).

[14]M. K. Cinibulk, G. Thomas, and S. M. Johnson, "Oxidation Behavior of Rare-Earth Disilicate–Silicon Nitride Ceramics," *J. Am. Ceram. Soc.*, **75** [8] 2044–9 (1992).

[15]H. Park, H.-E. Kim, and K. Niihara, "Microstructural Evolution and Mechanical Properties of $Si_3N_4$ with $Yb_2O_3$ as Sintering Additive," *J. Am. Ceram. Soc.*, **80** [3] 750–6 (1997).

[16]S. K. Lee and M. J. Readey, "Development of a Self-Forming Ytterbium Silicate Skin on Silicon Nitride by Controlled Oxidation," *J. Am. Ceram. Soc.*, **85** [6] 1435–40 (2002).

[17]H. Park, H.-W. Kim, and H.-E. Kim, "Oxidation and Strength Retention of Monolithic $Si_3N_4$ and Nanocomposite $Si_3N_4$–SiC with $Yb_2O_3$ as a Sintering Aid," *J. Am. Ceram. Soc.*, **81** [8] 2130–4 (1998).

[18]S. S. Chan and A. T. Bell, "Characterization of the Preparation of $Pd/SiO_2$ and $Pd/La_2O_3$ by Laser Raman Spectroscopy," *J Catal.*, **89**, 433–41 (1984).

[19]B. D. Meadowcroft, "Some Properties of Strontium-Doped Lanthanum Chromite," *Br. J. Appl. Phys.*, **2** [2] 1225–33 (1969).

[20]H. Klemm, C. Taut, and G. Wotting, "Long-Term Stability of Nonoxide Ceramics in an Oxidative Environment at 1500°C," *J. Eur. Ceram. Soc.*, **23**, 619–27 (2003).

[21]S. P. Taguchi and S. Ribeiro, "Silicon Nitride Oxidation Behavior at 1000°C and 1200°C," *J. Mater. Process. Techn.*, **147**, 336–42 (2004).

[22]F. F. Lange, S. C. Singhal, and R. C. Kuznicki, "Phase Relations and Stability Studies in the $Si_3N_4$–$SiO_2$–$Y_2O_3$ Pseudoternary System," *J. Am. Ceram. Soc.*, **60** [5–6] 249–52 (1977).

[23]A. Bellosi, G. N. Babini, L. P. Huang, and X. R. Fu, "Phase Effects on Oxidation Resistance in $Si_3N_4$–$Al_2O_3$–$Y_2O_3$," *Mater. Chem. Phys.*, **26**, 21–33 (1990).

[24]N. S. Jacobson and G. N. Morscher, "High-Temperature Oxidation of Boron Nitride: I, Monolithic Boron Nitride," *J. Am. Ceram. Soc.*, **82** [2] 393–8 (1999).

[25]N. S. Jacobson and G. N. Morscher, "High-Temperature Oxidation of Boron Nitride: II, Boron Nitride Layers in Composites," *J. Am. Ceram. Soc.*, **82** [6] 1473–82 (1999).

[26]C. G. Cofer and J. Economy, "Oxidative and Hydrolytic Stability of Boron Nitride—A New Approach to Improving the Oxidation Resistance of Carbonaceous Structures," *Carbon*, **33** [4] 389–95 (1995). □